Self-assembly of end-tethered nanorods in a neat system and role of block fractions and aspect ratio

Mark A. Horsch,[a] Zhenli Zhang[a] and Sharon C. Glotzer*[ab]

Received 24th August 2009, Accepted 24th November 2009
First published as an Advance Article on the web 6th January 2010
DOI: 10.1039/b917403f

We report a computational study of the self-assembly of end-tethered nanorods in a neat system (no solvent). We present morphological phase diagrams for low and moderate aspect ratio rods as a function of inverse temperature *vs.* relative tether fraction. Our simulations predict that the end-tethered rods self-assemble into hexagonally arranged chiral cylinders, hexagonally perforated lamellae, monolayer and bilayer arrowhead structures and wavy lamellae. For high aspect ratio tethered nanorods and small tether fractions, we observe that the tethered nanorods self-assemble into smectic and zig-zag lamellar morphologies.

Introduction

Rod-like nanoparticles are of particular technological importance due to their shape-anisotropy and nanometre scale dimensions. Computer simulations have predicted that by attaching tethers to precise locations on the surface of a nanoparticle, the nanoparticles can be induced to self-assemble into highly ordered structures.[1–11] In a previous study,[2–4] we investigated the self-assembly of tethered nanorods in a selective solvent for the rod. That study focused on the effects of concentration, rod aspect ratio, and relative tether fraction on the self-assembled structures. However, self-assembled structures formed in a neat system are important for many applications. It is, therefore, of interest to investigate the equilibrium structures accessible to polymer-tethered rods in a neat system. Toward this end we present morphological phase diagrams in the $1/T$ *vs.* relative coil fraction f_c plane for nanorods with aspect ratios of 3 : 1 and 5 : 1. Our studies predict that the tethered nanorods self-assemble into chiral cylinders, hexagonally perforated lamellar sheets, wavy lamellae, zig-zag lamellae and monolayer and bilayer arrowhead morphologies.

Rod–coil copolymers, one example of polymer-tethered nanorods, are known to exhibit many rich morphologies including smectic,[12–16] arrowhead,[17] zig-zag lamellar,[17] wavy lamellar,[17] bicontinuous,[12–14] double hexagonal cylinder,[16,18] and hexagonal cylinder morphologies.[12–15,19] The local packing of the rods in the above-mentioned morphologies is commonly unknown and subject to interpretation. For example, in the arrowhead phase[17] observed by Chen and Thomas it is not known if the rods form tilted bilayers or monolayers. To address the local packing of the rods Chen and Thomas proposed several packing models consistent with the dimensions of the observed morphology.

Until recently, theoretical studies of tethered rods have been limited to one and two dimensions. Matsen and Barrett[20] and Prymitsyn and Ganesan[21] presented one-dimensional phase diagrams for systems of rod–coil copolymers calculated using self-consistent field theory. Their studies primarily predicted smectic phases. Prymitsyan and Ganesan extended their work and presented a phase diagram for rod–coil copolymers in two dimensions.[21] For the two-dimensional rod–coil systems, they predicted smectic, bilayer arrowhead, and broken puck morphologies.[21] However, they were unable to examine the local packing of the rods within these structures and they were unable to predict the hexagonal cylinder phase. The first temperature *vs.* concentration phase diagram for a three-dimensional system determined by molecular simulations was reported by Horsch *et al.*[2] The phases predicted by our studies were in good agreement with those observed experimentally. For example, our simulations predicted the formation of tetragonally and hexagonally perforated lamellar phases, which had been observed experimentally[22] but which had not yet been predicted by theory or molecular simulation. Additionally, our studies predicted a novel hexagonal cylinder phase comprised of chiral cylinders.[2] Chen *et al.* presented the first three-dimensional inverse temperature *vs.* relative rod fraction phase diagram for tethered rods predicted by self-consistent field theory.[23] In their studies, self-consistent field theory was used to study the tethered rods, which to some extent allowed them to determine the local packing of the rods. The morphologies observed in their study were in good agreement with those observed experimentally[17,19,22,24] and those predicted by simulations,[2] although some differences exist. For example, they did not predict the formation of elongated micelles or the tetragonally perforated lamellar morphology. Recently, Reenders and Brinke using a Landau free energy functional with both a compositional and an orientational order parameter mapped a phase diagram for rod–coil block copolymers in terms of the Flory–Huggins parameter and relative rod fraction.[25] They predicted the formation of body centered cubic, hexagonal cylinder and lamellar structures for small rod volume fraction, and nematic and smectic C phases for large rod volume fraction.

In this study, we compare the inverse temperature, $1/T$, *vs.* relative tether fraction, f_c, phase behavior for high (14 : 1), moderate (5 : 1), and low (3 : 1) aspect ratio rods. For the

[a]*Department of Chemical Engineering, University of Michigan, Ann Arbor, Michigan, 48109-2136, USA. E-mail: sglotzer@umich.edu*
[b]*Department of Materials Science & Engineering, University of Michigan, Ann Arbor, Michigan, 48109-2136, USA*

moderate and low aspect ratio rods, we present the morphological phase diagrams in the $1/T$ *vs.* relative coil fraction, f_c, plane. Our simulations predict that the aspect ratio of the rods strongly influences the self-assembled morphologies formed by the tethered rods. For example, high aspect ratio rods are observed to form zig-zag lamellar morphologies, whereas moderate and low aspect ratio rods form smectic C morphologies for similar coil fractions. The manuscript is outlined as follows. First, we briefly describe the model and simulation method. Second, we present the $1/T$ *vs.* f_c phase behavior of low aspect ratio rods. Next, we present the $1/T$ *vs.* f_c phase behavior for moderate aspect ratio rods. Then, we briefly study high aspect ratio rods and the zig-zag morphology, and lastly, we discuss the results.

Model and method

We model the rods as a series of N_{rb} beads linked rigidly in a linear geometry,[1] see Fig. 1. The beads are permanently frozen together and the rod is treated as a rigid object. The rods used in our study are not intended to represent a specific chemistry but are intended to capture the universal behavior of rod-like particles permanently connected to a flexible tether, where the size of the tether is of the order of the size of the rod for all aspect ratios. The flexible tethers are modeled as linear, bead-spring chains comprised of N_{tb} beads bonded together *via* a finitely extensible, nonlinear, elastic (FENE) spring.[26] The relative tether fraction f_c is hence defined as $f_c = N_{tb}/(N_{tb} + N_{rb})$. To study the self-assembly of the tethered rods in a neat system, we implement attractive interaction potentials between like species and repulsive potentials between unlike species. Specifically, inter- and intra-tether and inter-rod non-bonded interactions are modeled by a 12-6, site–site Lennard-Jones (LJ) potential truncated and shifted to zero at $r_C = 2.5\sigma$. Non-bonded rod–tether interactions are treated with a purely repulsive Weeks–Chandler–Andersen (WCA) potential. The WCA potential is the LJ potential truncated at the minimum and shifted vertically by the well depth.

The length and energy scales for these systems are σ and ε, respectively, and the time unit is $\tau = \sigma\sqrt{m/\varepsilon}$, where m is the mass of a bead, $\sigma = \sigma_{TT} = \sigma_{RR} = \sigma_{RT}$ are the diameters of the beads, and $\varepsilon = \varepsilon_{TT} = \varepsilon_{RR} = \varepsilon_{RT}$ are the interaction parameters. The subscripts TT, RR, and RT correspond to tether–tether, rod–rod, and rod–tether, respectively. The inverse dimensionless temperature is in units of ε/k_BT. To compare the phase behavior between low and moderate aspect ratio rods, we rescale the inverse temperature by N_{rb}, akin to the rescaling of the Flory–Huggins χ parameter to compare self-assembled phases for copolymers of varying degrees of polymerization.

Brownian dynamics (BD) is used to study the tethered rod system. In BD, the trajectory of each "bead" is governed by the Langevin equation and is subjected to conservative, random and drag forces, respectively. The drag coefficient is set to 1.0, thereby limiting the ballistic motion of a "bead" in a time step to less than 1.0σ. The random force is Gaussian with zero mean and obeys the fluctuation dissipation theorem. The combination of the random and viscous forces helps to minimize numerical round off errors that occur over long simulation runs. The stationary solution to the Langevin equation is the Boltzmann distribution and therefore these simulations sample the canonical (NVT) ensemble.

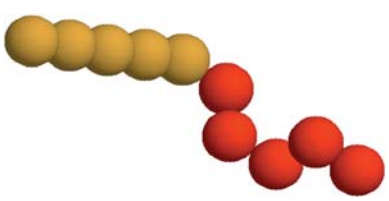

Fig. 1 Rendering of model tethered nanorod.

The rotational degrees of freedom of the rod are incorporated using the equations for rotation of linear bodies.[27] To integrate the equations of motion we employ the leapfrog integration algorithm. The time step Δt used to integrate the discretized equations of motion is 0.01τ. All simulations are initially carried out in a cubic cell with periodic boundary conditions. Systems are equilibrated athermally (repulsive interactions only) and subsequently cooled to the target temperature by decrementing the temperature in steps of $\Delta T = 0.01$. To ensure that the self-assembled structures are independent of the cooling history several different cooling rates are tested. To avoid system size effects, we consider systems of $N_R = 600$, 1000, 1600, 8192, and 12 800 corresponding to $N = 2400$–256 000 depending on the degree of polymerization of the tether beads, where N_R is the number of rods and N the total number of coarse-grained beads in the system. We also employ the box search algorithm to allow the shape of the box to change during the course of the simulation.[28] For the work presented in this manuscript, the box lengths are adjusted every five simulation steps.

Results

Self-assembly of low aspect ratio tethered rods

We define low aspect ratio rods as rods with an aspect ratio of 3 : 1. In Fig. 2, we present the morphological phase diagram, in the

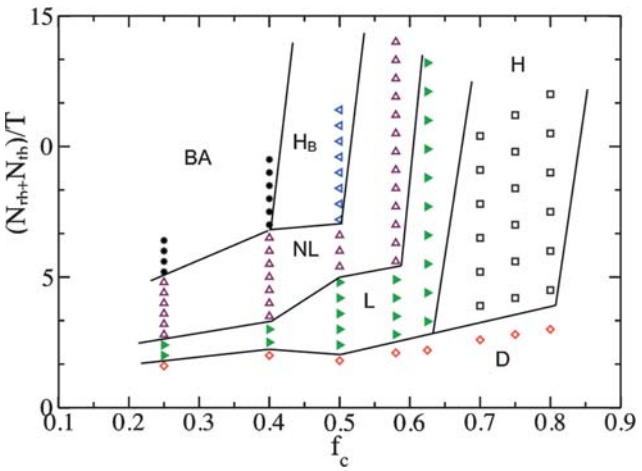

Fig. 2 Morphological phase diagram for low aspect ratio tethered rods. Black circles, upward pointing maroon triangles, left pointing blue triangles, right pointing green triangles, and black squares denote the bilayer arrowhead (BA), nematic lamellar (NL), hexatic B (H_B), lamellar (L), and hexagonal cylinder morphologies (H), respectively. The red diamonds denote the disordered state (D).

$1/T$ *vs.* f_c plane, for low aspect ratio rods. The solid lines in the phase diagram are used as guides to the eye to indicate where regions of ordered phases are observed and represent estimated phase boundaries. The simulations reveal that low aspect ratio tethered rods self-assemble into two distinct bilayer arrowhead phases, a lamellar phase with no orientational ordering in the rod layers, a nematic lamellar phase, a hexatic B phase, and a hexagonal cylinder phase. These phases are discussed in the following sections.

High tether fractions, $f_c \geq 0.7$. At high tether fractions, the elastic energy of the tether dominates and structures with curved interfaces form to reduce the elastic strain of the tethers. Fig. 3 is a typical simulation snapshot for a system of $N_R = 1600$ tethered rods at $N_{rb}/T = 12.0$, and $f_c = 0.8$. The snapshot reveals that the tethered rods self-assemble into a hexagonally arranged cylinder morphology. Within the cylinders the rods lack orientational order (see Fig. 3b) as determined by a nematic order parameter[4] whose value we calculate to be $S = 0.08 \pm 0.01$, where S ranges from zero to one. The lack of order within the cylinders is similar to that predicted for flexible amphiphiles and is in contrast to what is observed for higher aspect ratio rods. The rods within the cylinder form a circular cross-section, see Fig. 3c. To illustrate the packing of the tethers an individual cylinder is extracted from the simulation box and shown in Fig. 3c. The snapshot shows that the tethers extend radially from the cylindrical cores and the cylinders interact uniformly in a direction perpendicular to the cylindrical axis.

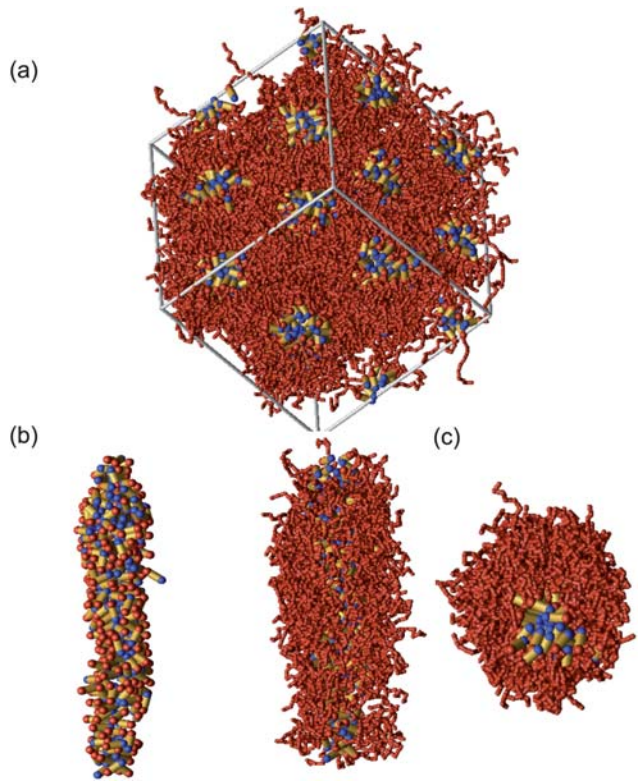

Fig. 3 Hexagonal cylinder morphology for a system of $N_R = 1600$ tethered rods, at $N_{rb}/T = 12.0$, and $f_c = 0.8$. (a) Snapshot of simulation cell showing hexagonal packing of the cylinders. (b) Individual cylinder extracted from the simulation cell in (a). The rod ends with tethers attached are colored red and those without tethers are colored blue. The tethers have been removed to illustrate the local packing of the rods within the cylinder. (c) Individual cylinder extracted from the simulation cell in (a). The left image is a side view and the right a face view of the cylinder, illustrating the cylindrical shell formed by the tethers around the rods.

Moderate tether fractions, $0.4 < f_c < 0.7$. For coil fractions similar to that of the rod fraction, the rod–rod interactions become important and structures with flat interfaces are preferred. Our simulations predict three distinct lamellar morphologies: a lamellar morphology with no orientational ordering of the rods, a lamellar morphology with nematic ordering of the rods, and a lamellar morphology with hexatic ordering of the rods. For $0.6 < f_c < 0.7$, the rods self-assemble into simple lamellar structures with no orientational ordering of the rods. For these tether fractions the nematic order parameter, S, is independent of temperature for the range of temperatures studied in this work. Within a rod layer, the rods pack randomly and S is calculated to be 0.072 ± 0.21. For tether fractions between 0.5 and 0.6 the tethered rods assembled into a simple lamellar morphology below $N_{rb}/T \approx 5.0$ and a nematic lamellar morphology above $N_{rb}/T \approx 7.0$. Fig. 4a is a typical simulation snapshot for a system of $N_R = 2400$ tethered rods, for $f_c = 0.58$, at $N_{rb}/T = 7.0$. The snapshot reveals that the rods self-assemble into lamellar sheets. Fig. 4b is a snapshot of the simulation cell in Fig. 4a taken normal to the lamellar sheet. In this snapshot the orientational ordering of the rods within a sheet is clear. To quantify the ordering within the sheet we plot the nematic order parameter as a function of temperature, see Fig. 4c. A sharp increase in the order parameter from $S \approx 0.08$ to $S \approx 0.35$ is observed at $N_{rb}/T = 5.0$. The increase is indicative of a transition from a random state to a nematic phase. Above $N_{rb}/T = 5.0$, the nematic order parameter is independent of temperature for the range of temperatures studied in this work. This suggests that the excluded volume of the tether is significant in determining the local packing of the rods.

For smaller tether fractions $0.4 < f_c < 0.58$, the simple lamellar, nematic lamellar and hexatic B lamellar structures are predicted for increasing values of N_{rb}/T. Fig. 5 is a simulation snapshot of a system of $N_R = 1600$, at $N_{rb}/T = 12.0$ for $f_c = 0.5$. A single sheet extracted from the simulation cell is presented in Fig. 5b. Within the sheets the rods have six first neighbors and white lines are drawn to illustrate the consistency of the preferred directions between neighbors. The long-range directional order is consistent with a hexatic B phase. In contrast to the nematic lamellar phase observed at lower values of N_{rb}/T, the degree of orientational ordering is much greater in the hexatic B phase. Fig. 5c is a plot of the nematic order parameter as a function of temperature. Two distinct increases appear in the nematic order parameter corresponding to the transitions from the simple lamellar to the nematic lamellar morphology and from the nematic lamellar to the hexatic B lamellar morphology. The high degree of orientational ordering and the temperature dependence of the order parameter suggest the importance of the rod–rod interactions in determining the self-assembled structure.

Small tether fractions, $f_c \leq 0.4$. For small tether fractions, the rod–rod interactions dominate and structures with flat interfaces

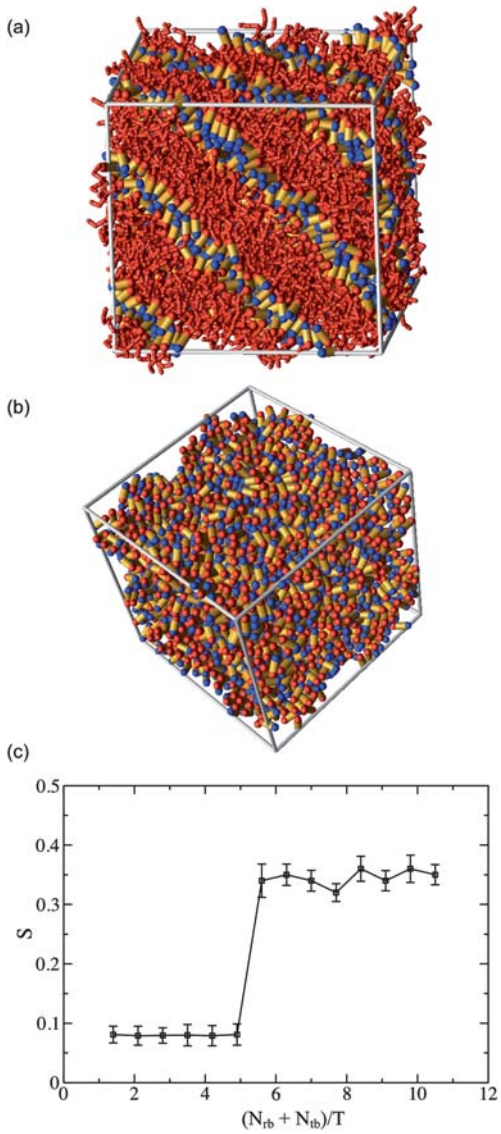

Fig. 4 Simulation snapshots of the nematic lamellar morphology, for a system of $N_R = 2400$ tethered rods, at $N_{rb}/T = 7.0$. (a) Side view of simulation cell illustrating the lamellar morphology. (b) View of simulation cell normal to lamellar sheets. Tethers have been removed for visualization of the rod packing. Rod ends with tethers attached are colored red and those without tethers are colored blue. (c) Plot of nematic order parameter for a system of tethered rods with an aspect ratio of 3 : 1 at $f_c = 0.58$.

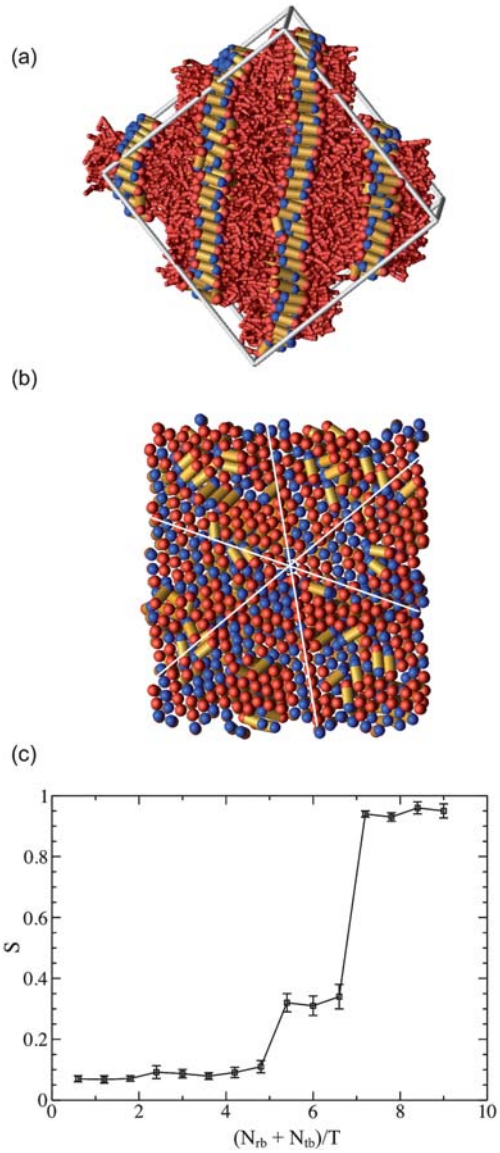

Fig. 5 Simulation snapshot of hexatic B lamellar morphology for $N_R = 1600$ tethered rods, at $N_{rb}/T = 12.0$ for $f_c = 0.5$. (a) Side view of simulation cell revealing lamellar morphology. (b) Single sheet extracted from the simulation cell in (a). White lines show preferred neighbor directions. Rod ends with tethers attached are colored red and those without tethers are colored blue. (c) Plot of nematic order parameter for a system of tethered rods with an aspect ratio of 3 : 1 for $f_c = 0.5$.

are preferred. For N_{rb}/T below approximately 3.0, simple lamellar structures are predicted with no orientational ordering of the rods within a sheet. For N_{rb}/T between approximately 3.0 and 7.0, nematic lamellar phases are predicted. Similar to the nematic lamellar morphologies formed at higher tether fractions, the nematic order parameter is $S \approx 0.08$ to $S \approx 0.36$. As N_{rb}/T is increased to above 5.0 for $f_c = 0.25$ and 7.0 for $f_c = 0.4$, the system undergoes a phase transformation from nematic lamellar, where the rods form monolayer sheets, to a bilayer arrowhead morphology. By forming bilayers the interfacial area between the rods and the tethers is decreased by a factor of two. However, the decrease in interfacial area results in an increase in the density of the tether–rod anchor points and an entropic penalty is suffered for stretching the tether. The simulations predict the formation of two distinct bilayer, arrowhead phases.

The first of the arrowhead phases is illustrated in Fig. 6a for a system of $N_R = 8192$, at $N_{rb}/T = 5.6$ for $f_c = 0.25$. The snapshot reveals several levels of ordering. The first level of ordering is the hexagonal packing of the rods within an individual layer, Fig. 6b. The second level of order arises from the packing of two smectic C monolayers, which are essentially mirror images, to form a v-shaped bilayer. The third level of ordering is the alternating direction of the v-shaped patterns between neighboring bilayers as illustrated in Fig. 6a. Lastly, the bilayers arrange to form

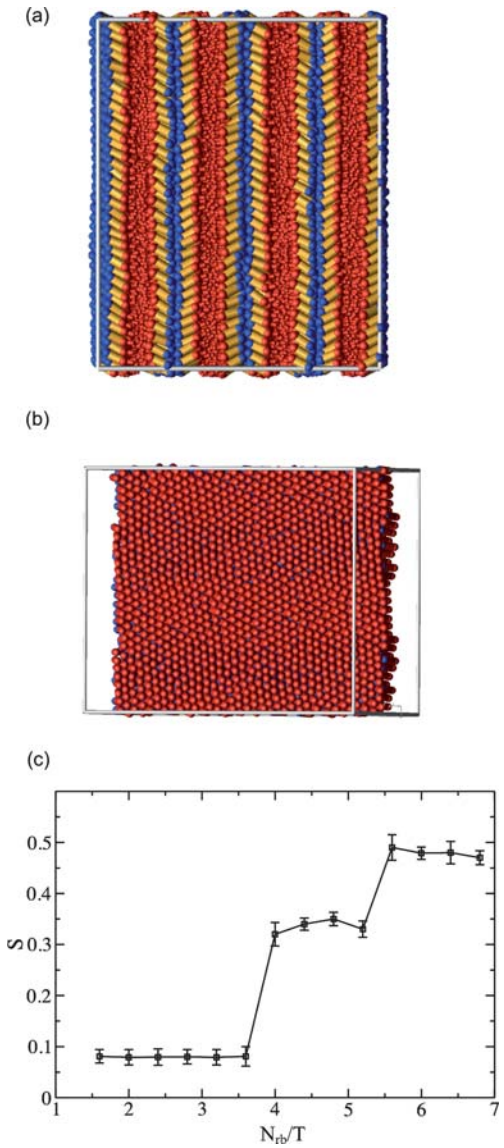

Fig. 6 Simulation snapshot of a bilayer arrowhead morphology for a system of $N_R = 8192$ tethered rods, at $N_{rb}/T = 5.6$ for $f_c = 0.25$. (a) Simulation cell illustrating both the v-shaped pattern formed by the rods comprising the bilayer and the alternating direction of the v-shaped pattern between neighboring bilayers. (b) Single sheet extracted from the simulation cell in (a). The tethers have been removed to allow visualization of the rod packing within the bilayer. (c) Plot of the nematic order parameter for a system of tethered rods with a rod aspect ratio of 3 : 1, at $f_c = 0.25$.

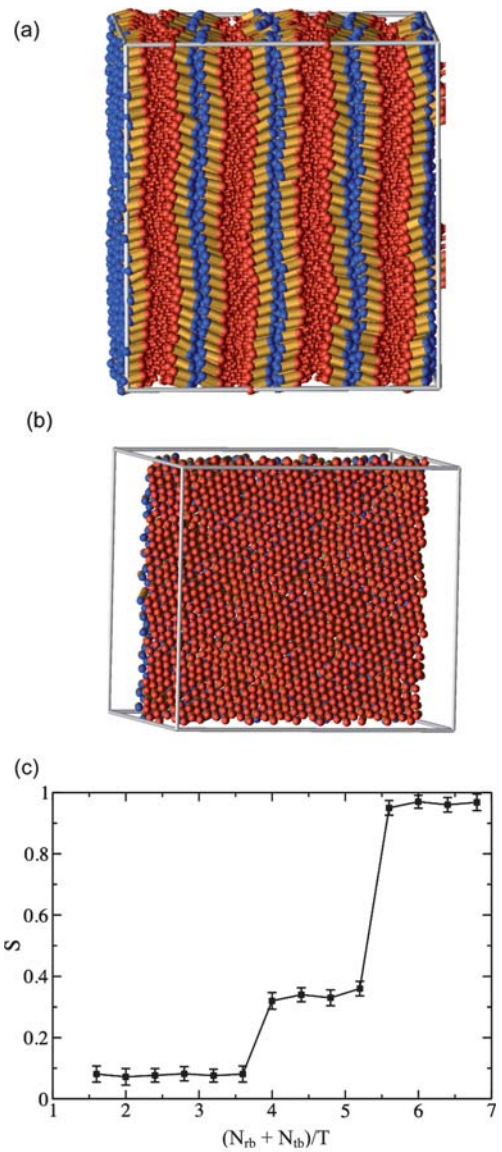

Fig. 7 Simulation snapshot of bilayer arrowhead phase for a system of tethered rods with a rod aspect ratio of 3 : 1 and $f_c = 0.25$. (a) Simulation cell illustrating the linear packing of the rods within the bilayer and the alternating directions of the neighboring bilayers. (b) Individual sheet extracted from the simulation cell in (a). The tethers have been removed for visualization of the rod packing. (c) Plot of the nematic order parameter for a system of tethered rods with a rod aspect ratio of 3 : 1, at $f_c = 0.25$. The large increase in the nematic order parameter at $N_{rb}/T = 5.6$ corresponds to the transition from the nematic lamellar phase to the bilayer arrowhead phase shown in Fig. 10.

a lamellar morphology wherein the bilayers are separated by a layer of tethers. The nematic order parameter is plotted as a function of temperature in Fig. 6c. Two distinct jumps in the order parameter are observed. The first increase corresponds to the transition from simple lamellae to nematic lamellae and the second from nematic lamellae to the bilayer arrowhead phase. As shown in the figure, there is only a small increase in the nematic order parameter between the nematic and bilayer phase. The increase is small due to the relative orientation of the two monolayers that make up the bilayers.

The second arrowhead phase is illustrated in Fig. 7 for a system of $N_R = 8192$, $f_c = 0.25$, and $N_{rb} = 5.6$. This is at the same state point as the first arrowhead phase and represents the first polymorphic state point we observed. As in the first bilayer arrowhead phase, several levels of ordering are observed. The first level is again the hexagonal packing of the rods within the bilayer (Fig. 7b). The second level of ordering arises from the packing of two smectic C monolayers into the bilayer. Unlike the bilayer phase illustrated in Fig. 6, the monolayers comprising the bilayer are not mirror images and a linear alignment of the rods between the two monolayers is predicted. The third level of ordering arises from the alternating direction of the smectic C bilayers such that

two neighboring bilayers form a v-shaped pattern. Lastly, the bilayers and tethers arrange to form a lamellar morphology with alternating layers of tethers and bilayers. The nematic order parameter for the system shown in Fig. 7a,b is plotted in Fig. 7c. Again, two sharp increases are observed in the order parameter. The first corresponds to the transition from the simple lamellae to the nematic lamellar morphology and the second corresponds to the nematic lamellae to bilayer arrowhead transition. Because the rods between monolayers in the bilayer are aligned, there is a significant increase in the nematic order parameter at the transition from nematic lamellae to bilayers. Within the bilayers the rods pack into a hexagonal crystal arrangement. The crystalline order of the rods within the bilayers is illustrated by the individual sheet extracted from the simulation cell. A similar bilayer smectic structure has been observed experimentally by Li *et al.* in which the rod segments align with the bilayer normal, *i.e.* a smectic A morphology.[29]

To ensure that the bilayer arrowhead phases are not a result of finite size effects, eight additional runs were performed using the box search algorithm, which allows the sides of the box to change length[28] subject to the constraint of constant volume. No distinguishable differences are observed for the spacing or energy per rod between the different runs. As described above, two distinct bilayer arrowhead phases form for the same coil fractions and inverse temperatures. A comparison between the two different arrowhead phases shows that the potential energy per rod is -0.89 ± 0.08 and -0.91 ± 0.09 for the first and second arrowhead phases, respectively. The formation of two different morphologies at the same state point leads to the question as to which morphology is the lowest free energy or if they are degenerate states. Since we are unable to easily determine the free energy difference between the two morphologies this question remains open. However, we find that both morphologies readily form with approximately the same frequency of occurrence. Although the bilayer arrowhead phases are reminiscent of chiral smectic phases formed by bent-core liquid crystals,[30,31] the formation of the v-shaped patterns in this study results from the consideration of adjacent rod monolayers or bilayers and not from the geometry of individual building blocks as in bent-core molecules.

Self-assembly of moderate aspect ratio tethered rods

We define moderate aspect ratio rods as those with an aspect ratio of 5 : 1. The morphological phase diagram in the N_{rb}/T *vs.* f_c plane is presented in Fig. 8. The solid lines are estimated phase boundaries and are guides to illustrate where ordered phases are observed. Our simulations reveal that tethered rods with moderate aspect ratios self-assemble into smectic A and C phases, a hexatic B phase, a monolayer arrowhead phase, a wavy lamellar structure, hexagonally arranged chiral cylinder phases, and a hexagonally perforated phase. The phases are discussed in the following sections.

High tether fractions, $f_c \geq 0.65$. At high tether fractions the elastic energy of the tether is the dominant interaction and morphologies with curved interfaces are formed. For $f_c > 0.65$, two distinct cylinder morphologies are predicted. At $f_c > 0.7$, the cylinders form with a circular cross-section, while at lower tether

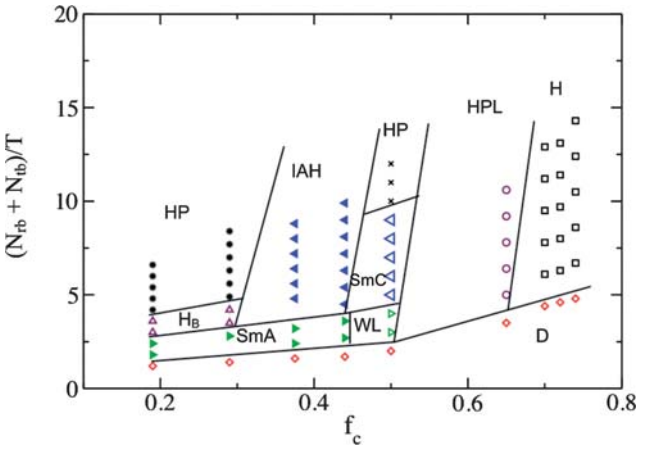

Fig. 8 Morphological phase diagram for tethered rods with a rod aspect ratio of 5 : 1. Black stars, upward maroon triangles, and rightward filled green triangles denote crystal (HP), hexatic B (H_B), and smectic A (SmA) phases respectively. Blue leftward filled triangles, blue leftward unfilled triangles, green rightward unfilled triangles, and black crosses denote interdigitated arrowhead (IAH), smectic C (SmC), wavy lamellae (WL), and lamellae with two-dimensional crystalline packing within the layer (HP). The maroon circles and black squares denote the hexagonally perforated lamellar (HPL) and hexagonal cylinder morphologies (H) respectively. The red diamonds denote the disordered state (D).

fractions the cylinders form with an ellipsoidal cross-section. Fig. 9a is a simulation snapshot for a system of $N_R = 2000$ tethered rods at $N_{rb}/T = 9.5$ for $f_c = 0.74$. The snapshot reveals that the tethered rods self-assemble into cylindrical structures that are hexagonally arranged. Within the cylinders the rods pack in an interdigitated manner to relieve the elastic strain of the tethers. The interdigitation of the rods is illustrated in Fig. 9b by the red and blue rod ends. The red ends represent rod ends with tethers attached and the blue represent rod ends without tethers. To further release the elastic strain, the rods form a twist along the cylindrical axis and thus the cylinders are chiral. However, since the cylinders are separated by the tether corona, their chirality is uncorrelated and randomly distributed, and the system is racemic. As mentioned earlier the cross-section of the cylinder is circular and is illustrated in Fig. 9c. The circular cross-section is significant in that the compressibility of the tether corona is approximately uniform perpendicular to the long axis of the cylinder. Therefore, the most efficient packing of the cylinders is in a hexagonal arrangement.

Fig. 10a is a simulation snapshot for a system of $N_R = 2000$, at $N_{rb}/T = 8.5$ for $f_c = 0.7$. In contrast to the cylinders formed at tether fractions of 0.74 where the cylinders are hexagonally arranged, the cylinders illustrated in Fig. 10 have a rectangular or rhombohedral packing and their cross-section exhibits C_{mm} symmetry. The rods pack in an interdigitated fashion within the cylinders as in the case of the cylinders formed at higher tether fractions. The red and blue rod ends, defined above and shown in Fig. 10b, illustrate the interdigitated packing. The cross-sectional area of the cylinders is ellipsoidal in contrast to the circular cross-section formed at higher tether fractions. This anisotropic cross-section results in an anisotropic tether corona illustrated in Fig. 10c. The anisotropy in the cylinder shape manifests as anisotropic interactions between neighboring cylinders for which

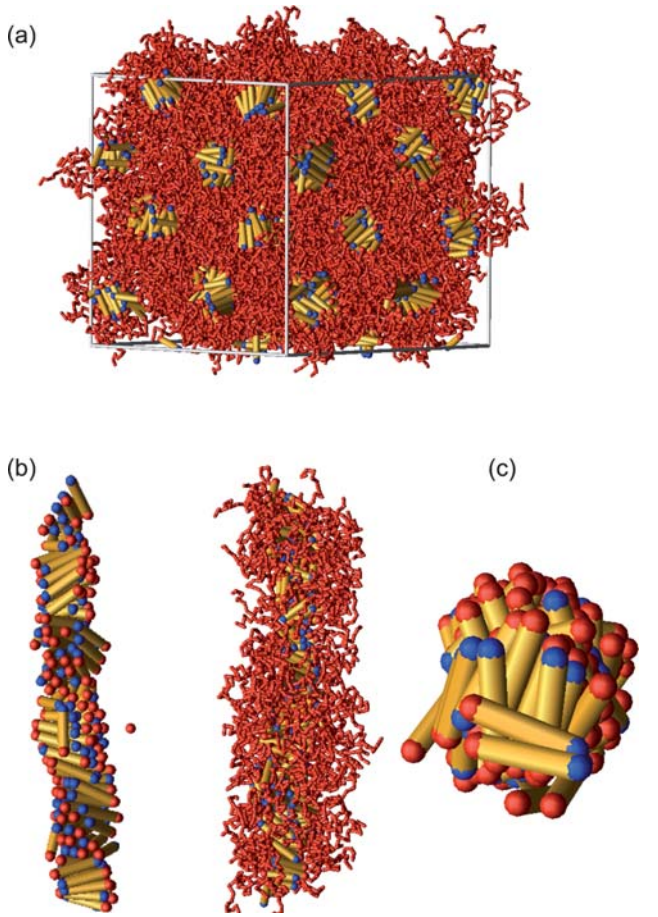

Fig. 9 Simulation snapshot of a hexagonal cylinder morphology for a system of $N_R = 2000$ tethered rods of aspect ratio 5 : 1, at $N_{rb}/T = 9.5$ and $f_c = 0.74$. (a) Snapshot of simulation cell illustrating hexagonal packing of the cylinders. (b) Single cylinder extracted from the cell in (a) to visualize the twist along the cylindrical axis, without tethers (left) and with tethers (right). Rod ends with tethers attached are colored red and those without tethers are blue. (c) Cylinder in (b) rotated to illustrate the circular cross-section of the cylinder.

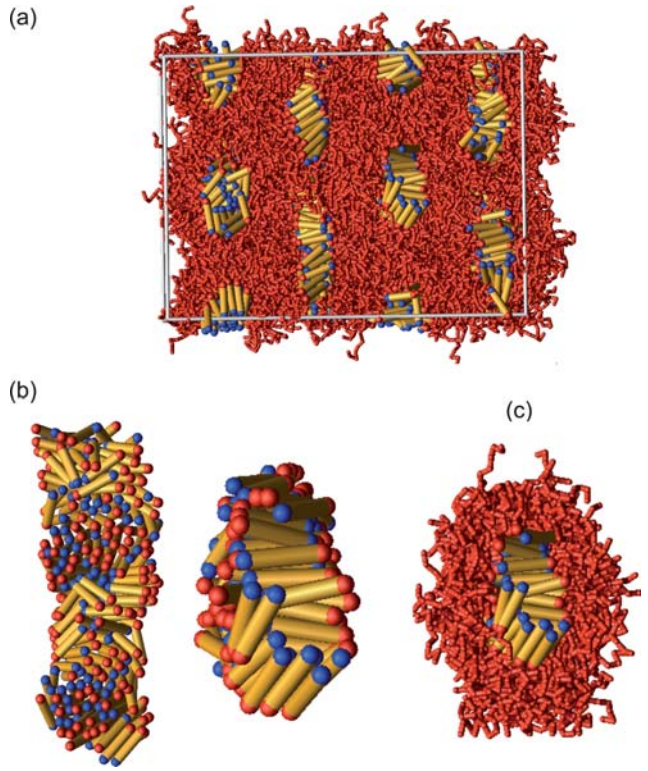

Fig. 10 Simulation snapshot of a centered rectangular cylinder morphology for a system of $N_R = 2000$ tethered rods of aspect ratio 5 : 1, at $N_{rb}/T = 8.5$ and $f_c = 0.7$. (a) Snapshot of simulation cell illustrating rectangular packing of the cylinders. (b) Single cylinder extracted from the cell in (a) to visualize the twist along the cylindrical axis. Rod ends with tethers attached are colored red and those without tethers are colored blue. (c) Cylinder in (b) rotated to illustrate the circular cross-section of the cylinder, without tethers left and with right.

the most efficient packing of the cylinders is centered rectangular or rhombohedral.

For $f_c = 0.65$, the simulations predict that the rods self-assemble into a hexagonally perforated lamellar morphology. The perforated lamellar morphology is a compromise between the hexagonal cylinder morphology observed at higher tether fractions and the smectic lamellar morphologies observed at a lower tether fraction. In addition to the ordered perforations within a layer, the perforations between layers stack in an ABAB pattern and the structure is periodic in three dimensions. Fig. 11 is a simulation snapshot of a system of $N_R = 12\,800$ tethered rods for $N_{rb}/T = 8.5$ and $f_c = 0.65$. The snapshots in Fig. 11b,c illustrate the hexagonal packing of the perforations and the ABAB stacking between layers. The snapshots further reveal the packing of the tethers into holes and the subsequent ordering of the holes into a hexagonal pattern.

Moderate tether fractions, $0.25 < f_c \leq 0.5$. As the tether fraction is further decreased, the rods self-assemble into sheet structures. For equal tether and rod fractions our simulations predict wavy lamellar, smectic C and crystalline phases. Fig. 12a is a simulation snapshot of $N_R = 1600$ tethered rods with $f_c = 0.5$ and $N_{rb}/T = 3.5$. The snapshot illustrates the wavy lamellar morphology. This morphology has been observed experimentally and predicted theoretically for one-, two- and three-dimensional systems.[17,21,23,32] However, it is not clear from these studies if the wavy lamellar phase is an equilibrium structure or a metastable structure. In the one-dimensional theoretical predictions, the zig-zag lamellar morphology was shown to be independent of the underlying lattice and the periodic boundary conditions.[32] In the two-dimensional theoretical predictions, the wavy lamellar phases changed under annealing suggesting that the structures are not an equilibrium phase. However, it is not clear whether or not the third dimension is important in the stability of this structure. In the three-dimensional theoretical predictions, the wavy lamellar morphology was shown to have a higher free energy than a simple lamellar phase.[23] Additionally, the phase was shown to be unstable if the rods were aligned perpendicular to the zig-zag direction and evolved to the lamellar morphology when the rods were assumed to be perfectly parallel within the sheet.[23]

Interestingly, our simulations predict the formation of the zig-zag or wavy lamellar morphology for similar tether fractions as those in the three-dimensional theoretical work.[23] However, in

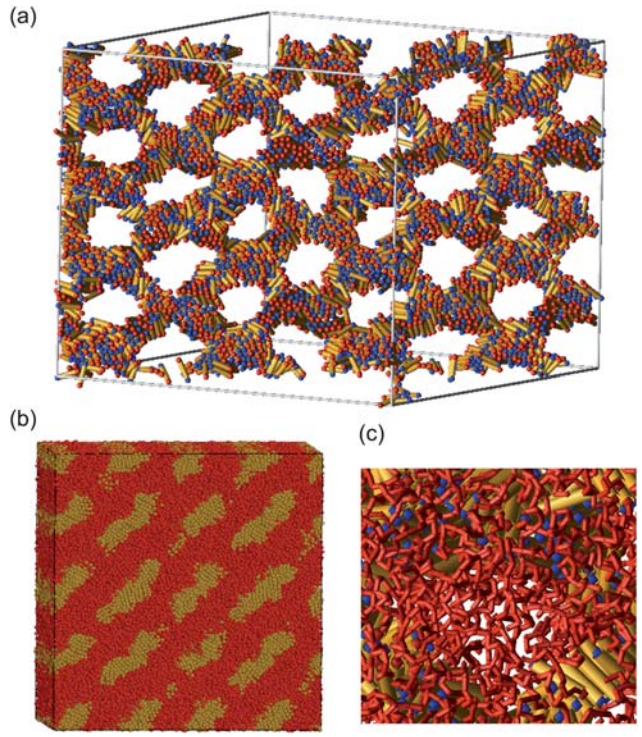

Fig. 11 Simulation snapshot of the hexagonally perforated lamellar morphology for a system of $N_R = 12\,800$ tethered rods, at $N_{rb}/T = 8.5$ and $f_c = 0.65$. (a) Snapshot of a single sheet in the simulation cell with the tethers removed for visualization of the perforations. Rod ends attached to tethers are colored red and those not attached are blue. (b) Side view of simulation cell. Tethers and rods have been rendered as beads to illustrate the ABAB packing between layers. Rods are colored gold and tethers red. (c) Close up of a single hole from the sheet in (a) with the tethers included to illustrate the packing of the tethers into the holes.

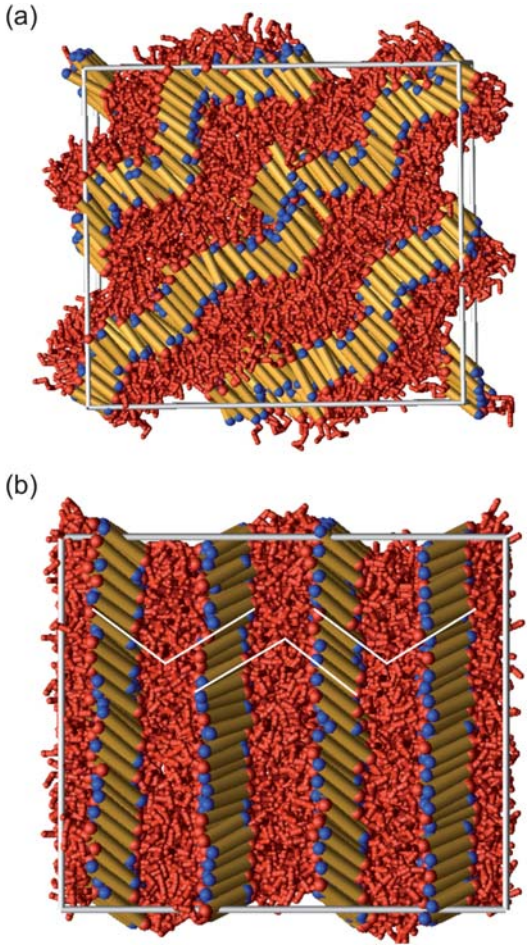

Fig. 12 Simulation snapshot of (a) the wavy lamellar morphology and (b) simulation snapshot of the interdigitated arrowhead morphology. The white lines denote the v-shaped patterns formed by neighboring rod layers.

our studies the alignment of the rods is not an input and was therefore not fixed during the course of the simulation. The lack of this constraint allows the rods to reorient within the sheet. The nematic order parameter of the rods within the sheets is calculated to be $S = 0.92 \pm 0.13$ indicating a high degree of alignment but not perfect alignment. The small degree of orientational freedom may stabilize this structure. Irrespective of whether the zig-zag or wavy lamellar phase is an equilibrium morphology, it has been observed in theory, simulation, and experiment suggesting that it is at least a metastable state.

For $0.375 \leq f_c \leq 0.44$, our simulations predict an interdigitated arrowhead morphology. Fig. 12b is a typical simulation snapshot for a system of $N_R = 1600$, $f_c = 0.44$ and $N_{rb}/T = 10.0$. The snapshot reveals that the tethered rods self-assemble into a lamellar structure where the rods pack into monolayer sheets. Interestingly, a mirror plane exists between neighboring sheets and a v-shaped pattern is formed, similar to the v-shaped morphology predicted for low aspect ratio rods. Within the lamellar structure, neighboring layers of rods alternate direction such that the neighboring "v" patterns alternate direction, see white lines in Fig. 12b. The formation of v-shaped patterns has not been previously observed for lamellar structures where the rods are arranged in monolayers. An open question remains as to why the v-shaped patterns form, since the correlation between rod monolayers is weak due to the thick tether layers between them and the short range of the rod–rod interactions.

Small tether fractions. For $0.19 \leq f_c < 0.3$, smectic A, hexatic B, and crystalline phases are predicted by our simulations. The high degree of alignment within each of these phases indicated by $S > 0.9$ suggests that the rod–rod interactions are dominant. However, there is a distinct absence of bilayer phases for the moderate aspect ratio tethered rods. The lack of bilayer phases here is interesting because the tether fractions are smaller for the moderate aspect ratio rods than for the low aspect ratio rods and should therefore have less influence on the self-assembled structure. This suggests that in addition to the decrease of rod–tether interfacial area, there must be another driving force for the formation of bilayers. We suggest two possible sources for this driving force. The first is entropic and arises from the stretching of the tether. For the low aspect ratio rods, there is more orientational freedom within the sheet-like structures than for the moderate aspect ratio rods. We postulate that this additional orientational freedom can result in a cooperative effort wherein the particles pivot to reduce the elastic strain of the tethers. The second driving force we propose is energetic and is believed to

arise from the rod–rod interaction range relative to the length of the rod. In the case of the low aspect ratio rods, the rod–rod interaction range is similar to the length of the rod, while the rod–rod interaction range is only half the rod length for the moderate aspect ratio rods. Therefore the small rods not only decrease their rod–tether interface by packing in bilayers, but they also increase the number of neighbors within their interaction range. The moderate aspect ratio rods also decrease the rod–tether interface but there is only a slight increase in the number of neighbors within their interaction range. Therefore, the bilayers are only observed for simulations of low aspect ratio rods.

Self-assembly of high aspect ratio rods

To investigate high aspect ratio rods we choose rods with an aspect ratio of 14 : 1. This size rod was chosen based on its inability to form a disordered structure at melt densities. For these large rods, a comprehensive study of the phase behavior is not computationally feasible. However, we are able to investigate long rods with small tether fractions. The desire of the long rods to align parallel to each other results in the formation of smectic morphologies and a zig-zag lamellar morphology. Fig. 13a is a simulation snapshot of $N_R = 2592$ tethered rods for $f_c = 0.17$, at $N_{rb}/T = 1.8$. The snapshot reveals that the rods self-assemble into a zig-zag lamellar morphology. As the temperature is decreased the zig-zag structure rearranges and forms a smectic C lamellar morphology, see Fig. 13b. The zig-zag morphology has been observed experimentally for high aspect ratio rods, however, it was unclear as to whether or not it is an equilibrium structure or a metastable structure. Our simulations demonstrate that the zig-zag lamellae can rearrange as the temperature of the system is decreased suggesting that the zig-zag morphology is not a kinetically arrested structure but instead metastable to the lower T smectic C lamellar morphology. Interestingly, the zig-zag morphology has regions of smectic A and smectic C phases, see Fig. 13c, and may be a compromise between these phases.

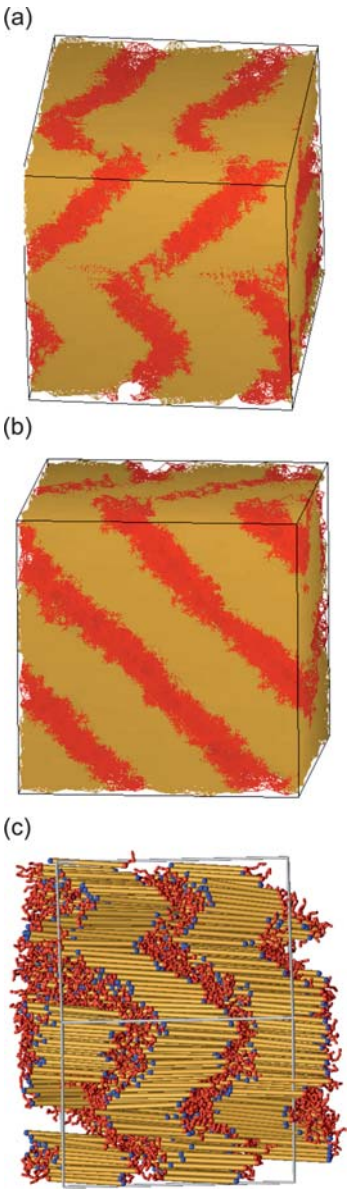

Fig. 13 Simulation snapshots of zig-zag lamellar and smectic C lamellar morphologies for a system of $N_R = 2592$ tethered rods of aspect ratio 14 : 1 for $f_c = 0.17$. The rods and tethers have been rendered as surfaces of constant density for viewing ease. The gold domains are the rods and the red domains the tethers. (a) Zig-zag morphology formed at $N_{rb}/T = 1.8$. (b) Smectic C lamellar morphology formed at $N_{rb}/T = 5.4$. (c) Zig-zag morphology in (a) rendered with rods and rotated to illustrate the smectic A and smectic C regions of the sheet.

Discussion

Our simulations predict that for low aspect ratio rods (3 : 1), the rods self-assemble into lamellar structures with no orientational ordering of the rods within the rod layers at high temperatures and nematically ordered rods at lower temperatures. For low temperatures, the rods form two distinct arrowhead phases. Bilayer arrowhead phases have been observed experimentally for rod–coil copolymers with a small coil fraction and a long rod[33] but not for small rods. The local packing of the rods within the experimentally observed arrowhead phases is not ascertainable but two packing models were proposed. The first packing model consists of bilayers formed by linear arrangements of rods forming a smectic C bilayer where between neighboring bilayers a mirror plane exists such that the neighboring bilayers form a v-shaped pattern. This model packing is identical to the packing observed for the bilayer arrowhead phase illustrated in Fig. 7a. The second packing model proposes that the rods pack into interdigitated, smectic C monolayers. The monolayers alternate in direction creating a mirror plane between neighboring monolayers. The neighboring monolayers form a v-shaped pattern. This suggested model packing is identical to that predicted by our simulations of moderate aspect ratio rods (see Fig. 12b). The lack of bilayers observed for the moderate aspect ratio rods suggests that in addition to lowering the interfacial energy another driving force is required for the formation of bilayers to offset the entropic penalty of increasing the elastic strain of the tether.

For moderate aspect ratio rods (5 : 1) in addition to the smectic phases predicted, we observe the formation of an interdigitated arrowhead structure discussed above, a wavy lamellar structure, a hexagonally perforated lamellar structure, and two distinct

cylindrical structures. The wavy and zig-zag lamellar morphologies observed for rod–coil copolymers have been argued to be non-equilibrium structures arising from the copolymers being "frozen" (unable to diffuse) by the removal of solvent. The change in the wavy lamellar morphology toward a smectic phase as the temperature is decreased suggests that the wavy lamellar structure is not a kinetically arrested structure. Further, this structure is obtainable from both a disordered state upon cooling and a smectic C phase upon heating. For high tether fractions cylinder structures are observed. The cylinders change from cylinders with a circular cross-section to cylinders with an ellipsoidal cross-section as the tether fraction is decreased. The change in the cross-sectional shape results in two different packings of the cylinders. Cylinders with circular cross-sections pack into a hexagonal morphology and those with ellipsoidal cross-sections pack into a rectangularly centered cubic or rhombohedral packing. We point out that this is consistent with the general trend toward surfaces with less curvature as the tether fraction decreases. As the tether fraction is further decreased, a hexagonally perforated lamellar structure is observed. This structure has been observed experimentally,[22] by simulation,[2] and recently by theory[23] for rod–coil copolymers.

For high aspect ratio rods (14 : 1), we observe the formation of the zig-zag and smectic morphologies. We show that as the temperature is decreased, the rods rearrange to form a lamellar structure suggesting that the zig-zag morphology is not a kinetically arrested structure. We propose that this structure is a compromise between the smectic A and smectic C morphologies. However, simulations of high aspect ratio rods are computationally expensive and an in-depth investigation is not within the scope of this work.

The success of the "minimal" model used in our study in predicting phases observed by both theory and experiment provides strong evidence as to the universal behavior of tethered rod systems. Our simulations provide considerable insight into the local packing of the rods within the self-assembled morphologies that should be of interest to both experimentalists and theoreticians.

Acknowledgements

This work was supported by the US Department of Energy under grant DE-FG-02-02ER46000. We are grateful to Trung Dac Nguyen for his assistance with the manuscript.

References

1 Z. L. Zhang, M. A. Horsch, M. H. Lamm and S. C. Glotzer, *Nano Lett.*, 2003, **3**, 1341.
2 M. A. Horsch, Z. L. Zhang and S. C. Glotzer, *Phys. Rev. Lett.*, 2005, **95**, 056105.
3 M. A. Horsch, Z. L. Zhang and S. C. Glotzer, *J. Chem. Phys.*, 2006, **125**, 184903.
4 M. A. Horsch, Z. L. Zhang and S. C. Glotzer, *Nano Lett.*, 2006, **6**, 2406.
5 C. R. Iacovella, M. A. Horsch, Z. Zhang and S. C. Glotzer, *Langmuir*, 2005, **21**, 9488.
6 E. R. Chan, X. Zhang, C. Y. Lee, M. Neurock and S. C. Glotzer, *Macromolecules*, 2005, **38**, 6168.
7 X. Zhang, E. R. Chan and S. C. Glotzer, *J. Chem. Phys.*, 2005, **123**, 184718.
8 X. Zhang, Z. Zhang and S. C. Glotzer, *Nanotechnology*, 2007, **18**, 115706.
9 T. D. Nguyen, Z. Zhang and S. C. Glotzer, *J. Chem. Phys.*, 2008, **129**, 244903.
10 C. R. Iacovella and S. C. Glotzer, *Nano Lett.*, 2009, **9**, 1206.
11 A. J. Crane, F. J. Martínez-Veracoechea, F. A. Escobedo and E. A. Muller, *Soft Matter*, 2008, **4**, 1820.
12 M. Lee, B.-K. Cho, H. Kim and W.-C. Zin, *Angew. Chem., Int. Ed.*, 1998, **37**, 638.
13 M. Lee, B.-K. Cho, H. Kim, J. Y. Yoon and W.-C. Zin, *J. Am. Chem. Soc.*, 1998, **120**, 9168.
14 J.-H. Ryu and M. Lee, *Struct. Bonding (Berlin)*, 2008, **128**, 63.
15 B. D. Olsen and R. A. Segalman, *Macromolecules*, 2006, **39**, 7078.
16 L. R. N. Sary, C. Brochon, G. Hadziioannou, J. Ruokolainen and R. Mazzenga, *Macromolecules*, 2007, **40**, 6990.
17 J. T. Chen and E. L. Thomas, *Macromolecules*, 1995, **28**, 1688.
18 H. A. Klok, J. F. Langenwalter and S. Lecommandoux, *Macromolecules*, 2000, **33**, 7819.
19 L. H. Radzilowski, B. O. Carragher and S. I. Stupp, *Macromolecules*, 1997, **30**, 2110.
20 M. W. Matsen and C. Barrett, *J. Chem. Phys.*, 1998, **109**, 4108.
21 V. Pryamitsyn and V. Ganesan, *J. Chem. Phys.*, 2004, **120**, 5824.
22 M. Lee, B.-K. Cho, K. J. Ihn, W.-K. Lee, N.-K. Oh and W.-C. Zin, *J. Am. Chem. Soc.*, 2001, **123**, 464.
23 J.-Z. Chen, C.-X. Zhang, Z.-Y. Sun, Y.-S. Zheng and L.-J. An, *J. Chem. Phys.*, 2006, **124**, 104907.
24 M. Lee, B.-K. Cho and W.-C. Zin, *Chem. Rev.*, 2001, **101**, 3869.
25 M. Reenders and G. Brinke, *Macromolecules*, 2002, **35**, 3266.
26 G. S. Grest and K. Kremer, *Phys. Rev. A*, 1986, **33**, 3628.
27 M. P. Allen and D. Tildesley, *Computer Simulations of Liquids*, Oxford University Press, U. S. A., 1987.
28 A. J. Schultz, C. K. Hall and J. Genzer, *J. Chem. Phys.*, 2004, **120**, 2049.
29 C. Y. Li, K. K. Tenneti, D. Zhang, H. Zhang, X. Wan, E.-Q. Chen, Q.-F. Zhou, A-.O. Carlos, S. Igos and B. S. Hsiao, *Macromolecules*, 2004, **37**, 2854.
30 R. A. Reddy and C. Tschierske, *J. Mater. Chem.*, 2006, **16**, 907.
31 W. Weissflog, H. N. Shreenivasa Murthy, S. Diele and G. Pelzl, *Philos. Trans. R. Soc. London, Ser. A*, 2006, **364**, 2657.
32 W. Li and D. Gersappe, *Macromolecules*, 2001, **34**, 6783.
33 J. T. Chen, E. L. Thomas, C. K. Ober and G.-p. Mao, *Science*, 1996, **273**, 343.

